Marine Geodesy

ISSN: 0149-0419 (Print) 1521-060X (Online) Journal homepage: http://www.tandfonline.com/loi/umgd20

Kinetic Energy Variability in the North Indian Ocean Using a Numerical Model

Aftab A. Can & Raj Kumar Sujit Basu

To cite this article: Aftab A. Can & Raj Kumar Sujit Basu (2002) Kinetic Energy Variability in the North Indian Ocean Using a Numerical Model, Marine Geodesy, 25:1-2, 175-186, DOI: 10.1080/014904102753516813

To link to this article: http://dx.doi.org/10.1080/014904102753516813

Published online: 10 Nov 2010.

Marine Geodesy, 25:175–186, 2002

0149-0419/02 $12.00 + .00

Kinetic Energy Variability in the North Indian Ocean Using a Numerical Model

AFTAB A. CAN

Department of Marine Sciences and Biotechnology
Goa University
Goa, India

RAJ KUMAR
SUJIT BASU

Oceanic Sciences Division
Meteorology and Oceanography Group
Space Applications Center
Ahmedabad, India

The North Indian Ocean exhibits profound impact of variation in lower tropospheric winds. In the present study climatological monthly winds are used to force a nonlinear reduced gravity model of the North Indian Ocean to simulate climatological surface circulation and sea level anomaly for all 12 months of the year. The sea level anomalies agree reasonably well with satellite altimeter derived sea level anomalies. The model successfully simulates the varying eddy structure and current pattern of the North Indian Ocean. Finally, the kinetic energy variation in the North Indian Ocean with special reference to equatorial region and the boundaries is analyzed in detail.

Keywords North Indian Ocean, numerical model, altimetry, kinetic energy

The North Indian Ocean is characterized by strong seasonal changes of circulation due to two opposite northeast and southwest monsoon regimes. The Somali Current flows northeastward during southwest monsoon and flows southwestward during the northeast monsoon. The gyre circulations in the Arabian Sea and Bay of Bengal reverse during these two monsoon regimes. The seasonal variations of the wind-driven circulation pattern in the North Indian Ocean is greater than that in any other ocean. Previous modeling studies of this ocean have generally been concerned mainly with Somali Current reversal and generation of gyres like The Great Whirl and the Somali Gyre in the northwestern Indian ocean during the onset of summer monsoon (Luther and O'Brien 1985; McCreary and Kundu 1988; Simmons et al. 1988; Kindle and Thompson 1989). Reversal of gyre circulation in the Bay of Bengal has also been studied (Potemra et al. 1991; Yu et al. 1992). McCreary et al. (1993) studied intrabasin teleconnections, focusing on the role of planetary waves in the Indian Ocean

Received 8 June 2001; accepted 16 October 2001.

The authors wish to express their deep gratitude to the Center for Space Science and Technology Education in Asia-Pacific, Dehradun, India, Space Applications Center, Ahmedabad, India. The first author is highly thankful to Prof. B. S. Sonde, Goa University, Goa, India. Thanks are also due to NASA, USA.

Address correspondence to Dr. A. A. Can, Department of Marine Sciences and Biotechnology, Goa University, Goa 403206, India. E-mail: askhan@unigoa.ernet.in

while Dube et al. (1990) studied the relationships between interannual variability in the Arabian Sea and summer monsoon rainfall. Perigaud and Delecluse (1992, 1993) analyzed Geosat altimeter data for comparisons with numerical simulations from the reduced gravity model forced by observed winds. Recently, Basu et al. (2000) performed a similar study using a reduced gravity model and compared the simulations with altimeter observations using the technique of empirical orthogonal functions. Singh et al. (2001) studied the impact of satellite altimetry on the simulations of sea level variability by an Indian Ocean model, and Tewari et al. (2000) demonstrated the use of satellite data in a model of the northwestern Indian Ocean.

Most of the studies mentioned above are concentrated on simulations of the current patterns. The present work aims at studying the kinetic energy associated with the currents in the equatorial wave-guide region and along the coast after validating the model-derived sea level anomalies. For this purpose a nonlinear reduced gravity model is utilized and is forced with climatological monthly winds obtained from Florida State University to simulate the sea surface height anomaly and surface circulation. The kinetic energy associated with the changing current structure is then estimated.

Model Description

The model describes the ocean as a system consisting of two layers. The upper layer rests on the lower layer, which is at rest, and the interface between the two layers is the approximation of pycnocline. The two layers are homogenous both vertically and horizontally. The density difference between the two layers is $\Delta\rho$, and ρ is the mean density. The hydrostatic and Boussinesq approximations are adopted.

The governing equations are described using spherical polar coordinates. The reduced gravity equations in transport form are:

$$\frac{\partial U}{\partial t}+\frac{1}{a\cos\theta}\frac{\partial}{\partial\phi}\left[\frac{U^2}{H}\right]+\frac{1}{a}\frac{\partial}{\partial\theta}\left[\frac{UV}{H}\right]-(2\Omega\sin\theta)\,V$$
$$=-\frac{g'}{2a\cos\theta}\frac{\partial H^2}{\partial\phi}+\frac{\tau^{\theta}}{\rho_1}+A\nabla^2U-\gamma U, \tag{1}$$

$$\frac{\partial V}{\partial t}+\frac{1}{a\cos\theta}\frac{\partial}{\partial\phi}\left[\frac{UV}{H}\right]+\frac{1}{a}\frac{\partial}{\partial\theta}\left[\frac{V^2}{H}\right]+(2\Omega\sin\theta)\,U$$
$$=-\frac{g'}{2a}\frac{\partial H^2}{\partial\theta}+\frac{\tau^{\varphi}}{\rho_1}+A\nabla^2V-\gamma V, \tag{2}$$

and

$$\frac{\partial H}{\partial t}+\frac{1}{a\cos\theta}\left[\frac{\partial U}{\partial\varphi}+\frac{\partial(V\cos\theta)}{\partial\theta}\right]=-\gamma\,(H-H_o). \tag{3}$$

$U=uH$ and $V=vH$ represent the eastward and northward components of the upper-layer transport, respectively; u and v are the depth independent eastward and northward velocity components in the upper layer. H is the upper layer thickness, ϕ and θ denote longitude and latitude, respectively, t is the time, $f(=2\Omega\sin\theta)$ is the coriolis parameter. Ω and a are the angular velocity and radius of the earth, respectively. A is horizontal eddy viscosity

(10000 $m^2 s^{-1}$) and g^l is the reduced gravity (0.03 m s^{-2}),

$$g^l = g\Delta\rho/\rho_1, \tag{4}$$

ρ_1 is the density of the upper layer (1023 kg m^{-3}), γ is the damper introduced to absorb incoming radiations at the eastern boundary. H_o is the initial upper layer thickness (200 m). The wind forcing (τ), is a body force acting over the upper layer,

$$\tau = \tau(\tau^\phi, \tau^\theta). \tag{5}$$

The model domain extends from 29°S to 23°N and 40°E to 119°E. However, the primary region of interest is the region north of 10°S. Verschell and others (1995) have shown that closing the passage to the Pacific Ocean does not significantly affect the circulation in the Northern Indian Ocean. The region south of 10°S is considered as sponge region. The wind has been damped in this region, using a cosine damper and the eddy viscosity has been increased (Basu et al. 1996). All the boundaries are closed with no-slip condition ($u = v = 0$). The southern and part of eastern boundary are open boundaries. However, no-slip condition is applied at these boundaries. To overcome the problem of southern open boundary, the analysis and results will be restricted to north of 10°S. Since no-slip boundary condition is applied at the entire eastern boundary, a damper is included near the eastern boundary that efficiently absorbs incoming radiation (McCreary and Kundu 1989). All the fields are damped near the eastern boundary. The damping coefficient γ, which is same for all the variables U, V, and H, is zero except within 2.5° of the open part of the eastern boundary, where it increases linearly to a distance of 1.5° and is constant thereafter. The maximum strength of damping is 1 day^{-1}. The horizontal resolution is 0.5° on an Arakawa C-grid in both latitudinal as well as longitudinal direction. The time step is 15 min.

On the surface the boundary condition is the wind stress. The component of the wind stress in x-direction is

$$\tau^x = \rho_a \, C_d \, \sigma_x, \tag{6}$$

and the component in y-direction is

$$\tau^y = \rho_a \, C_d \, \sigma_y, \tag{7}$$

where

$$\sigma_x = W_x \sqrt{W_x^2 + W_y^2} \tag{8}$$

and

$$\sigma_y = W_y \sqrt{W_x^2 + W_y^2} \tag{9}$$

are normally termed as pseudo stress components. Here, $C_d (= 1.3 \times 10^{-3})$ is the drag coefficient, ρ_a is the air density, and W_x and W_y are the components of wind velocity in x and y directions, respectively.

The model was spun up from rest using climatological monthly wind stress provided by Florida State University. It was run for six years to achieve a steady annual cycle. The

model was able to produce the climatologically known current patterns in the North Indian Ocean. However, the main aim of the present work is to study the kinetic energy variability after proper validation using satellite data. The satellite altimeter provides only sea levels. Due to their inaccuracies, sea level anomalies (deviation from long term average) are used for comparing with model results. Thus, we restrict ourselves to the description of the sea level anomalies produced by the model and refrain from describing monthly current fields produced by the model.

Sea Level Anomaly (SLA) from the Model

The dynamic response of the North Indian Ocean to the changing wind field is also manifested in the sea level anomalies. The sea level anomaly as obtained by forcing the model with climatological monthly Florida State University pseudo-wind stress is discussed. Further $1^\circ \times 1^\circ$ data of sea level anomalies from October 1992 to February 1995 procured from University of Texas are used to determine the average monthly sea level anomalies. These anomalies are then compared with the model results to ascertain the validity of the model. The model-derived monthly sea level anomalies are described below. Although simulations are carried out for all the months, results for July and January, representing summer and winter only, are produced below for the sake of brevity and only important intraseasonal variability is discussed.

Northern Summer Sea Level Anomaly Variation

The variations in sea level anomaly (SLA) during northern summer (June to September), represented by July, is characterized by positive and negative anomalies. Along the continental boundaries the sea level is lower than the offshore region (Figure 1a). This dip is associated with the upwelling that is stronger along the western boundary. The negative SLA seen along the west coast of India propagates offshore with advance of the season. This propagation is highest at the southern limits. The variation of SLA in Bay of Bengal is weaker than in Arabian Sea and depicts a dip off the east coast of India that weakens with advance of the season. From May to June, high sea level anomaly seen in the eastern part is found to propagate along the eastern boundary into Bay of Bengal. Prasanna Kumar et al. (1998) indicated such sea level variations. Perigaud and Delecluse (1993) attributed such propagation to Rossby waves. The open boundary at the southern region shows positive sea level anomaly. The central-western region of the southern boundary shows highest positive SLA. This anomaly is associated with the South Equatorial Current. The positive SLA off Somalia and Arabia indicates the anticyclonic circulation associated with the Great Whirl and Socotra Eddy. With the advance of the season (September), the variations in SLA depict the weakening and subsequent absence of the eddy. Using TOPEX/POSEIDON altimeter data, Gairola et al. (1998) have also detected the Great Whirl and Somali Gyre system in this region.

Northern Winter Sea Level Anomaly Variations

The winter season (December to March) is represented by January. The variations in SLA depict positive anomalies along the western boundary, the west coast of India, and the east coast of India, while at the eastern boundary negative signatures are evident (Figure 1b). The region off Somalia depicts a dip, suggesting cyclonic eddy whose western limb is associated with the equatorward flowing Somali current. All along the west coast of India higher sea levels, which are associated with poleward flow, are reported. In the Bay of Bengal the SLA is more negative at the eastern region than at the western region. With the advance of the season the negative anomalies seen off the east coast of India extend

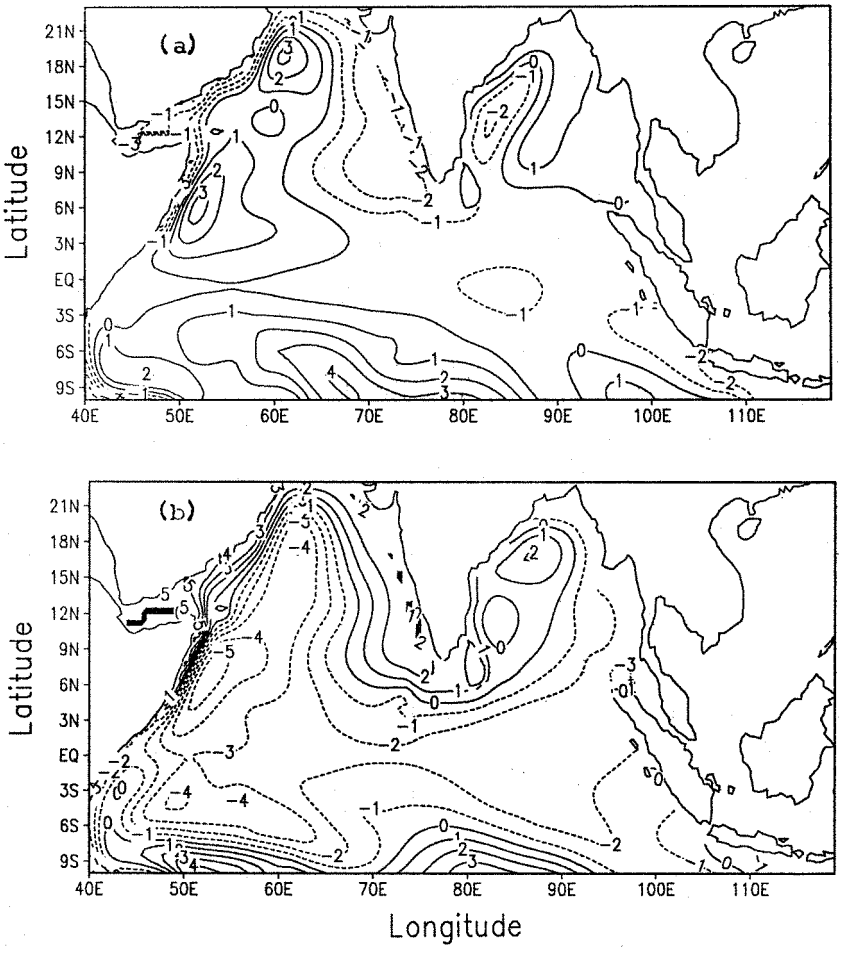

FIGURE 1 Model-derived sea level anomaly (cm) during July and January.

equatorward. At the equatorial region the negative anomaly is strongest at the west, while at the southern boundary the western region shows highest positive anomalies.

Validation of Model Results on Sea Surface Anomaly with Topex Data

In order to determine the mean monthly sea level anomalies the TOPEX sea level anomaly data, averaged from October 1992 to February 1995, is used to validate the model output. The TOPEX monthly sea level anomalies are presented in Figure 2. The varying sea level anomalies at the southern region are well in accordance with the TOPEX observations. At the equatorial region, the trends in the sea level anomalies obtained from the model agree well with the satellite data. Besides, the evolving high and low anomalies, which are associated with eddies and upwelling areas, are clearly depicted in both the model results and the TOPEX-derived sea surface height anomaly figures. The lower variability of the Bay of Bengal is also seen in the model results and the TOPEX data. The TOPEX data, however, do not agree well with the position of features like highs associated with eddies. This is perhaps due to a smaller period of TOPEX data that is used for averaging in order to find monthly averages.

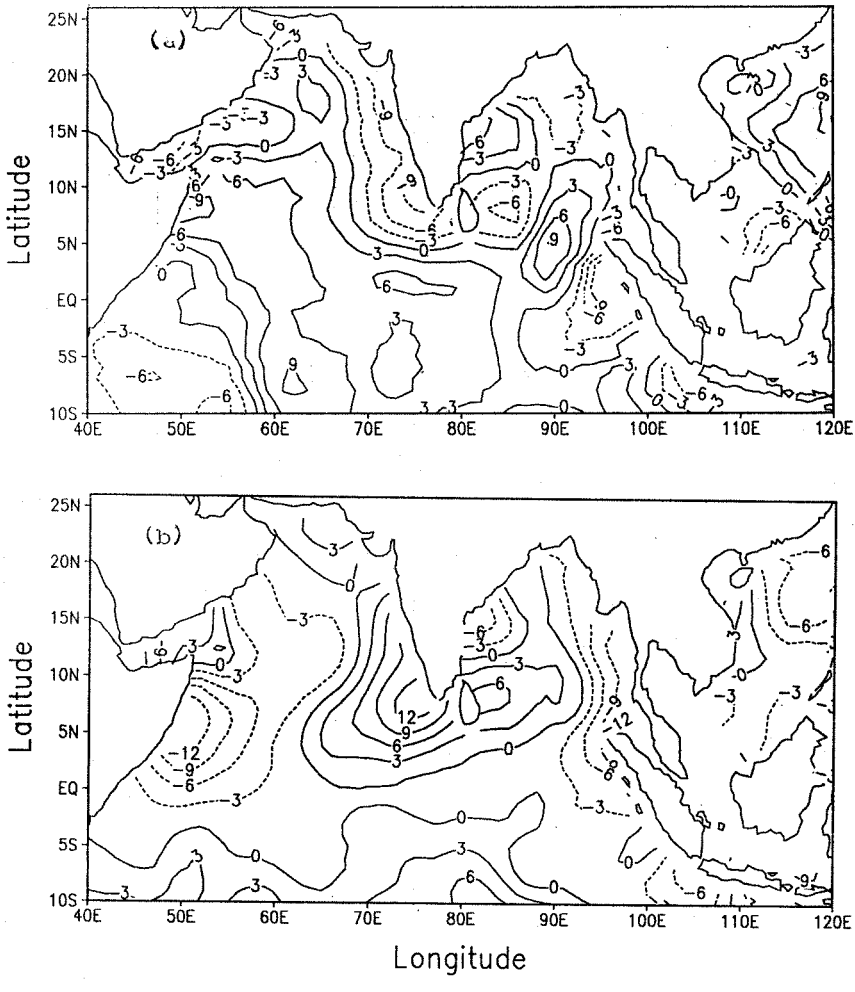

FIGURE 2 TOPEX-derived sea level anomaly (cm) during July and January.

Kinetic Energy Variability

The studies of kinetic energy ($(u^2 + v^2)/2$) variations of North Indian Ocean in response to seasons reveal the dynamic nature of the region. The spatial distribution of kinetic energy (KE) during the month of July (Figure 3a) reveals low KE and smaller variations in the eastern sector of the southern limit in comparison with the southwestern region. Along the Somalia coast, high KE is associated with the poleward Somali Current, but at the central equatorial region core of high is absent. In Bay of Bengal the KE is weak. With the advance of the season (September), the KE decreases.

During January, the entire region depicts a weak KE (Figure 3b). At the southwestern sector of the study area, the higher KE forms a prominent feature of January. From December to January, a decrease occurs. With further advance of the season (February), KE increases. In the central equatorial region, development of high KE is seen. In April, KE off Somalia is the least in the year. In general, low KE is seen in Arabian Sea and Bay of Bengal.

The kinetic energy spectrum of the region reveals that energy rich zones are associated with the major currents. To determine the KE variability associated with these currents, KE

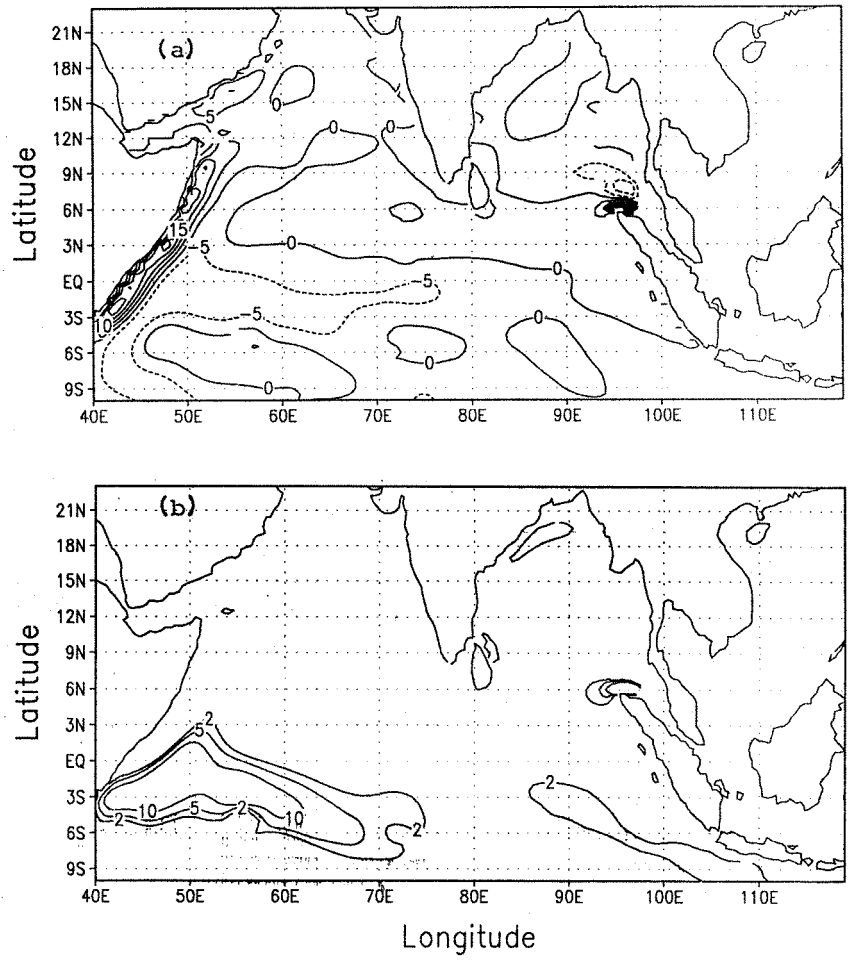

FIGURE 3 Kinetic Energy ($cm^2\ s^{-2}$) at the ocean surface during July and January.

in the equatorial wave guide region (5.5°N to 5.5°S), western rim of study region, and along the west and east coast of India are studied.

Kinetic Energy Variation in the Equatorial Wave-Guide Region (5.5°N to 5.5°S)

The equatorial wave-guide region of the Indian Ocean has remarkably different surface flow pattern during southwest monsoon than other similar regions of the world ocean. The whole equatorial wave-guide region is not covered by ocean. The region to the west of 49°E is partly land. Therefore, KE computed is less in that region. Hence, care is taken in interpreting the KE distribution.

In July (Figure 4), two peaks in the KE distribution are seen. The major one is associated with the northward limb of the Great Whirl, along the coast, and the weaker one with the southward limb. The manifestation of varying KE associated with the different limbs of Great Whirl is more prominent in July than June. The KE along the boundary decreases with further advance of the season. During January, concentration of energy at the western side occurs. However, over the rest of the region, the KE is found to be decreasing (Figure 4). The intensity is lower in January and the eastward extent of the region experiencing high

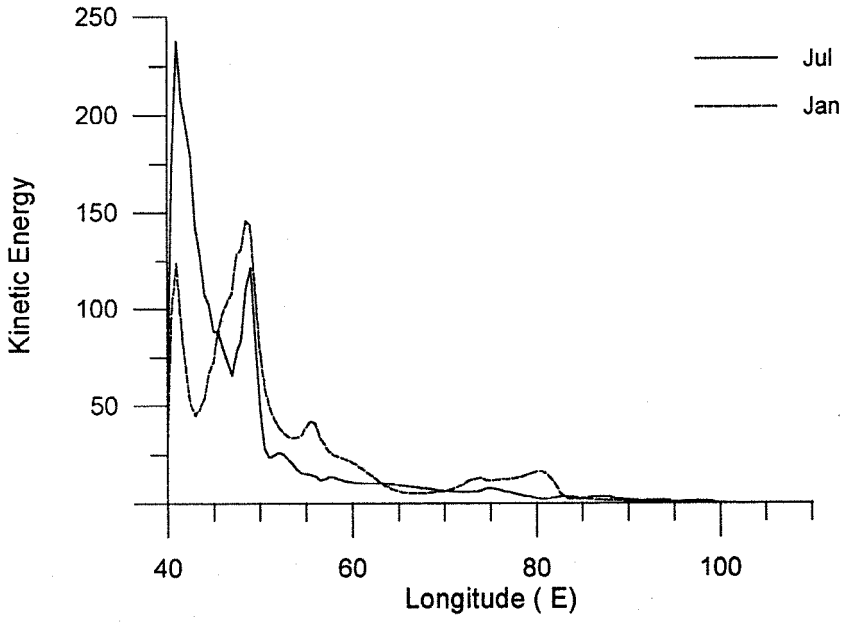

FIGURE 4 Kinetic Energy ($cm^2\ s^{-2}$) in equatorial wave-guide region during July and January.

energy is larger than that in July. In the later months of the season, a maxima develops at 70°E and propagates eastward.

Kinetic Energy Variation along the Western Boundary of Study Regime

The western boundary of Arabian Sea shows peculiar variations in the current pattern. The Somali Current (SC), which flows poleward in the northern summer, reverses in winter. Another interesting feature of this regime is the presence of eddies. The overall distribution of kinetic energy up to 2.5° from the western coast of the study region, during July and January, is shown in Figure 5.

During July, high KE associated with the poleward Somali Current is seen at the equatorial region of the western boundary towards north. It decreases drastically. Another peak is seen at 16°N, indicating the stronger currents off Arabia. The equatorial peak shifts northward and broadens, indicating poleward movement and widening of the Somali current from June to July. In the Later months of the season, the low latitude peak narrows and shifts northward, and subsequently the latitudinal extent decreases, indicating the weakening phase. In January, KE is weaker than in summer and shows a different pattern along the western margin (Figure 5). The energy distribution reveals two peaks. The first peak is associated with the southward moving Somali Current, and the second is due to current associated with northward flowing Zanzibar Current that is fed by South Equatorial Current. In February, the kinetic energy drastically decreases, and a single peak is seen at 2.5°N. In March, KE further decreases.

Kinetic Energy Variation along the West Coast of India

The KE variations along the west coast of India are less than those along the western boundary (Figure 6). During July, the KE shows drastic decrease between 7° and 8°N.

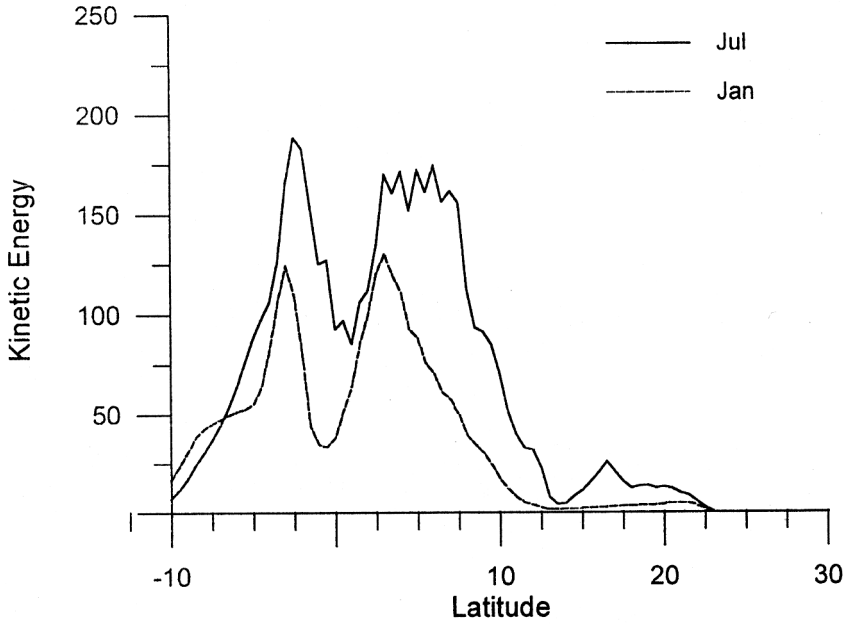

FIGURE 5 Kinetic Energy ($cm^2\ s^{-2}$) along the western boundary during July and January.

Northward of it, KE increases gradually. These variations weaken with the advance of the season, indicating the onset of summer to winter transition. In January, the KE variations depict a pattern similar to that in summer. The KE is associated with the poleward flow. The KE further decreases in the later months of the season.

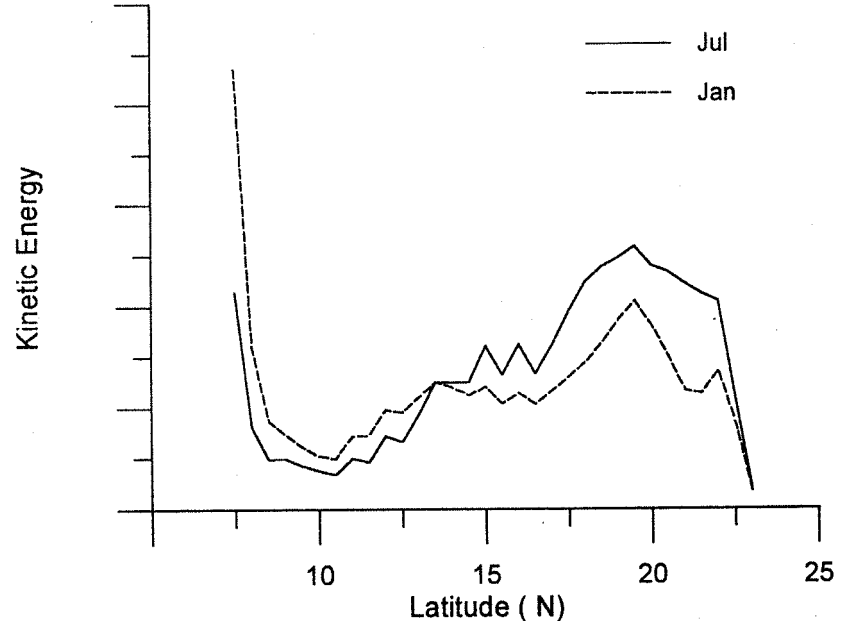

FIGURE 6 Kinetic Energy ($cm^2\ s^{-2}$) along the west coast of India during July and January.

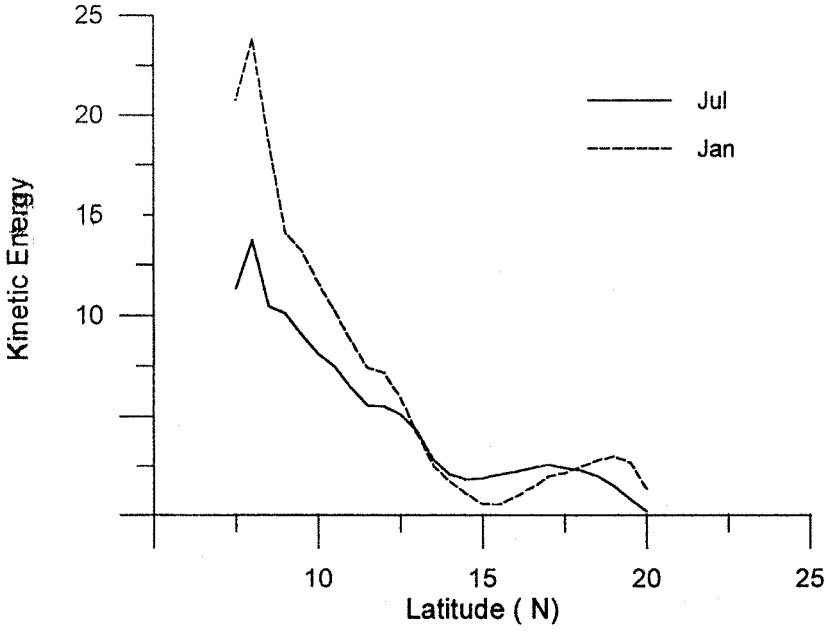

FIGURE 7 Kinetic Energy ($cm^2\ s^{-2}$) along the east coast of India during July and January.

Kinetic Energy Variation along the East Coast of India

The KE off the east coast of India is shown in Figure 7. During July and January, the KE decreases drastically up to 14°N and further north it gradually increases. The poleward increase is more pronounced in July. At the southern limit, the KE increases from August to September.

Conclusions

The model results show that the changing winds do not show simultaneous changes in the sea level anomaly over the entire North Indian Ocean. By mid April, the winds in Southern Hemisphere reverse and this reversal propagates northward. In general, north of South Equatorial Current, strong seasonal variations in magnitude and direction of currents are seen. The sea surface anomalies clearly indicate eddies and strong currents. Further, the model also shows the variation associated with Kelvin waves and Rossby waves.

The study shows that highest KE occurs in western region and is associated with eddies. Though the month of June is characterized by stronger winds, KE is not seen to be higher all over the study region. Further, in the central equatorial region, KE is found to decrease with respect to May. This indicates that the KE and, hence, the currents in the equatorial region are not primarily governed by the wind impulse. More advance models could give a better insight to the problem. Also, in the central Arabian Sea, KE increases from July to August. However, the winds are almost constant. This clearly indicates the lag in the response of the ocean surface to the wind forcing.

In the western part of the equatorial wave-guide region, the high KE at the west is partly due to the southward limb of Great Whirl and the Somali Current. During the southwest monsoon season, the Great Whirl is strong as indicated by high KE, and the KE in the rest of the region is found to be weak. This eddy is found to be developing in May, and it intensifies till July. From August to October it diminishes, and the KE in the central region and on the eastern region increases. From November to January the peak of KE broadens, indicating

intensification of the Somali current. The KE in the central and eastern regions does not decrease as seen during the southwest monsoon. Instead, it shows higher values further eastward from the Great Whirl due to the North Equatorial Current. The broad maxima in KE seen during the peak months of the two seasons (July and January) are an indication of matured eddy. The currents and the associated eddy are stronger in southwest monsoon than in northeast monsoon. The core of high KE moves poleward during southwest monsoon and back during northeast monsoon. The KE distribution indicates that the transition along the western rim of the study region is drastic from southwest to northeast monsoon, and from northeast to southwest it is gradual.

The lower KE along the west coast of India than that at the western rim reveals weaker currents. During the two seasons, the highest KE is seen off the southern coast and is associated with the equatorward and poleward flowing currents in summer and winter. These currents weaken drastically up to 10°N in summer and 13°N in winter. Further poleward, they increase. The KE off the east coast of India shows a decrease from July to September.

The study clearly shows the major current patterns and their variability associated with the atmospheric forcing. The evolution of eddies in the westernmost region and the change of direction is also seen. Further, the highest KE is found to be associated with eddies and the Somali Current. The sea level anomalies derived from the model are highly similar to the TOPEX sea surface height anomaly data. The anomalies indicate the propagation of Kelvin and Rossby waves. The energy pattern in equatorial wave-guide region shows concentration of energy on the westernmost region during the southwest monsoon. While in the transition and northeast monsoon period, the distribution at the central region is high. The KE off the coast indicates that the transition between the monsoons does not occur all over the study region at one time in response to the seasonal winds.

References

Basu, S., S. D. Meyers, and J. J. O'Brien. 2000. Annual and interannual sea level variations in the Indian Ocean from TOPEX/POSEIDON observations and ocean model simulations. *J. Geophys. Res.* 105:975–994.

Dube, S. K., M. E. Luther, and J. J. O'Brien. 1990. Relationships between interannual variability in the Arabian Sea and Indian summer monsoon rainfall. *Meteor. Atmos. Phys.* 44:153–156.

Gairola, R. M., S. Basu, P. C. Pandey, and T. C. Panda. 1998. Along track dynamical topography by Geosat, ERS-1 and TOPEX/POSEIDON altimeters with a new geoid model. *Indian J. Mar. Sci.* 27:17–25.

Kindle, J. C., and J. D. Thompson. 1989. The 26- and 50-day oscillations in the western Indian Ocean: Model results. *J. Geophys. Res.* 94:4721–4736.

Luther, M. E., and J. J. O'Brien. 1985. A model of seasonal circulation in the Arabian Sea forced by observed winds. *Prog. Oceanogr.* 14:353–385.

McCreary, J. P., and P. K. Kundu. 1988. A numerical investigation of the Somali current during the southwest monsoon. *J. Mar. Res.* 46:25–28.

McCreary, J. P., and P. K. Kundu. 1989. A numerical investigation of sea surface temperature variability in the Arabian sea. *J. Geophys. Res.* 94:16097–16114.

McCreary, J. P., P. K. Kundu, and R. L. Molinari. 1993. A numerical investigation of dynamics, thermodynamics and mixed layer processes in the Indian Ocean. *Prog. Oceanogr.* 31:181–244.

Perigaud, C., and P. Delecluse. 1992. Annual sea level variations in the southern tropical Indian Ocean from Geosat and shallow water simulations. *J. Geophys. Res.* 97:20169–20178.

Perigaud, C., and P. Delecluse. 1993. Interannual sea level variations in the tropical Indian Ocean from Geosat and shallow water simulations. *J. Phys. Oceanogr.* 23:1916–1934.

Potemra, J. T., M. E. Luther, and J. J. O'Brien. 1991. The seasonal circulation of the upper ocean in the Bay of Bengal. *J. Geophys. Res.* 96:12667–12683.

Prasanna Kumar, S., H. Sainath, P. Challenor, and H. T. Guymer. 1988. Seasonal and inter-annual sea surface height variations of the northern Indian Ocean from the TOPEX/POSEIDON altimeter. *Indian. J. Mar. Sci.* 27:10–16.

Simmons, R. C., M. E. Luther, J. J. O'Brien, and D. M. Legler. 1988. Verification of a numerical ocean model of the Arabian Sea. *J. Geophys. Res.* 93:15437–15453.

Singh, S. K., S. Basu, R. Kumar, and V. K. Agarwal. 2001. Impact of saltellite altimetry on simulations of sea level variability by an Indian Ocean model. *Marine Geodesy.* 24:53–63.

Tewari, K., R. Kumar, B. S. Gohil, and S. Basu. 2000. Use of ERS-1 scatterometer and TOPEX altimeter data in a nonlinear reduced gravity model of the northwestern Indian Ocean. *Indian. J. Mar. Sci.* 29:1–6.

Verschell, M. A., J. C. Kindle, and J. J. O'Brien. 1995. Effects of Indo-Pacific throughflow on the upper tropical Pacific and Indian Oceans. *J. Geophys. Res.* 100:18409–18420.

Yu, L., J. J. O'Brien, and J. Yang. 1992. On the remote forcing of the circulation in the Bay of Bengal. *J. Geophys. Res.* 96:20449–20454.